Author/s:
Truong, S;Huang, Y;Lang, F;Messmer, M;Simmonds, I;Siems, S;Manton, M

Title:
A Climatology of the Marine Atmospheric Boundary Layer over the Southern Ocean from Four Field Campaigns during 2016–2018

Date:
2020-10-27

Citation:
Truong, S., Huang, Y., Lang, F., Messmer, M., Simmonds, I., Siems, S. & Manton, M. (2020). A Climatology of the Marine Atmospheric Boundary Layer over the Southern Ocean from Four Field Campaigns during 2016–2018. Journal of Geophysical Research: Atmospheres, 125 (20), https://doi.org/10.1029/2020JD033214.

Formatted

A climatology of the marine atmospheric boundary layer over the Southern Ocean from four field campaigns during 2016 – 2018

S. C. H. Truong[1,3], Y. Huang[2,3], F. Lang[1], M. Messmer[2], I. Simmonds[2], S. T. Siems[1,3] and M. J. Manton[1]

[1]Monash University, Melbourne, Australia.

[2]The University of Melbourne, Melbourne, Australia.

[3]Australian Research Council Centre of Excellence for Climate Extremes (CLEX), Melbourne, Australia.

Corresponding author: Son Truong (son.truong@monash.edu)

Key Points:

- A climatology of the marine atmospheric boundary layer over the Southern Ocean is developed from four recent field campaigns.
- A multi-layer cloud structure is frequently observed in the vicinity of fronts and cyclones, particularly over the high latitudes.
- The upper level advection and detrainment of convection associated with mesocyclones are potential drivers of the multi-layer cloud coverage.

This is the author manuscript accepted for publication and has undergone full peer review but has not been through the copyediting, typesetting, pagination and proofreading process, which may lead to differences between this version and the Version of Record. Please cite this article as doi: 10.1029/2020JD033214

Abstract

A climatology of the marine atmospheric boundary layer (MABL) and the lower free troposphere over the Southern Ocean (SO) is constructed using 2186 high-resolution atmospheric soundings from four recent campaigns conducted in the period of 2016-2018. Relationships between the synoptic meteorology and MABL thermodynamic structure are examined using a *k*-means cluster analysis, complemented by front and cyclone composite analyses. Seven distinct clusters are identified, five of which are consistent with an established climatology over the SO storm track. Two new clusters (C1 and C2) are introduced over the high-latitude SO. C1 is commonly located poleward of the ocean polar front near mesocyclones, while C2 is located along the Antarctic coastline. A multi-layer cloud structure is frequently present in clusters in the vicinity of fronts and cyclones, while a single-layer coverage is more common in a suppressed environment, particularly at lower latitudes. A cloud-free, multi-level inversion is frequently observed in cluster C2, possibly linked to the descending, dry, katabatic winds off the Antarctic coast. A strong, primary inversion is typically present in clusters at lower latitudes with high mean sea level pressure. Across the SO storm track and higher latitudes (cluster C1), a multi-level inversion structure is also commonly observed. A preliminary analysis of two case studies suggests that upper level advection and detrainment of convection associated with mesocyclones are potential drivers of the multi-layer cloud coverage over the high-latitude SO rather than the decoupling mechanisms common in the subtropics.

1 Introduction

Cloud is one of the most critical factors in defining the regional radiation budget over the Southern Ocean (SO) (Haynes et al., 2011) and governing the meridional transport of energy and moisture from the tropics towards Antarctica (Zelinka and Hartmann 2012). However, large biases in the SO cloud amount and properties persist in both climate simulations and reanalysis products (Hyder et al., 2018; Schuddeboom et al., 2019). Trenberth and Fasullo (2010) attributed the SO shortwave radiation biases to the cloud amount, which is underestimated in the high latitudes in most general circulation models. Huang et al. (2012a,b) examined the SO clouds using multi-satellite products and detailed that the majority of SO clouds reside in the marine atmospheric boundary layer (MABL), where they are difficult to be accurately detected from space. Bodas-Salcedo et al. (2012) and Williams et al. (2013) reported that climate models struggled to produce low-level clouds, most notably behind cold fronts and/or in the cold-air sector of extra-tropical cyclones. At a larger scale, similar biases are found in the widely used reanalysis products such as the European Centre for Medium-Range Weather Forecasts Re-Analysis (ERA-Interim) and Modern-Era Retrospective analysis for Research and Applications reanalysis (Naud et al., 2014). It has been suggested that these biases are most likely attributable to deficiencies in the parametrization schemes, such as the cloud microphysics and the boundary layer schemes (e.g., Huang et al., 2014; Furtado and Field 2017).

Indeed, the understanding of the thermodynamic structure of the SO MABL remains a challenge owing to a lack of in situ observations. Williams et al. (2013) highlighted that the height of the SO MABL in the Transpose-Atmospheric Model Intercomparison Project simulation was consistently underestimated in comparison to an operational analysis product. When compared against historical atmospheric soundings over Macquarie Island, however, the height of the MABL in a reanalysis (ERA-Interim) product was itself underestimated [Hande et al., 2014; Lang et al., 2018 (hereafter referred to as L2018)]. The challenges in understanding the

SO MABL structure is also compounded by the common presence of multi-layer cloud within and beyond the MABL (e.g., Russell et al., 1998; Jensen et al., 2000; Mace et al., 2009; Chubb et al., 2016). Mace et al. (2009) examined the statistics of hydrometeor layers using the Cloudsat and CALIPSO observations; they emphasized that multiple low-level cloud layers appear to be present more frequently over the storm tracks and high latitudes of the SO than the North Pacific. This region can be seen to be spatially correlated with the largest biases in the SO shortwave radiation budget, which underscores the complexity of radiative transfer through multiple cloud layers and the ensuing heating/cooling rates. The multi-layer cloud is also well-documented over the Arctic (e.g., Vassel et al., 2019; Christensen et al., 2013; Liu et al., 2012), where it has been suggested that horizontal moisture and temperate advection is a key driving mechanism (Luo et al., 2008).

The presence of boundary layer decoupling, as recently reported in Mace and Protat (2018) and Zheng and Li (2019), adds further complication. Decoupling in the subtropics commonly occurs when a single well-mixed stratocumulus-capped boundary layer breaks down into two distinct well-mixed layers: a surface-flux driven sub-cloud layer and a turbulent cloud layer driven by radiative fluxes (e.g., Nicholls., 1983, Albrecht et. al., 1995; Bretherton and Wyant 1997; Jones et al., 2011). While the physical mechanism of the decoupled MABL were unexplored in Mace and Protat (2018), Zheng and Li (2019) investigated three cases and suggested that the commonly known "deepening-warming" decoupling mechanism (Bretherton and Wyant 1997), typically observed over the subtropics, is unlikely to occur over the SO. They further proposed that low-level warm air advection (LLWAA), where warm air advects over colder surface, is of potential importance.

Prompted by the need for a greater understanding of the clouds and boundary layer over the SO, four coordinated field campaigns were conducted over the Australian sector of the SO from 2016-2018, leading to an unprecedented collection of atmospheric measurements extending from Hobart Tasmania (43°S) to the edge of Antarctica (south of 65°S). Among these comprehensive measurements, 2186 high-resolution atmospheric soundings are available from these campaigns [the Clouds, Aerosols, Precipitation, Radiation, and Atmospheric Composition over the SO (CAPRICORN 2016, Mar – Apr 2016), and CAPRICORN 2018 (Jan – Feb 2018), the SO Clouds Radiation Aerosol Transport Experimental Study (SOCRATES, Jan – Feb 2018), the Measurements of Aerosols, Radiation, and Clouds over the SO Science Plan (MARCUS, Oct 2017 – Mar 2018), and the Macquarie Island Cloud and Radiation Experiment (MICRE/ACRE, Apr 2016 – Apr 2018)]. These soundings have been made from airborne, ship-based and ground-based platforms across the SO.

In this study, we employ these 2186 atmospheric soundings to develop a climatology of the marine atmospheric boundary layer over the SO. This climatology is done with the aid of a simple clustering algorithm. We examine the characteristics of the soundings as within the context of the synoptic meteorology, for example the distance from cyclone centres and meteorological fronts. In addition to the inversion height and cloud thickness, we examine features unique to the high-latitude maritime regions, such as the presence of multiple cloud layers and multiple inversions. Finally, we select two case studies from regions that are of great interest to the climate community, given their important role in defining the shortwave radiation budget over the SO which is poorly simulated in a multitude of climate models.

2 Data and Methodology

The data set consists of 2186 soundings taken over a period of 28 months (Jan 2016 – April 2018) from four independently-funded but coordinated field campaigns (Table 1). The domain of these field campaigns extending from north of Hobart to the coast of Antarctica (Fig. 1a).

Table 1. Overview of atmospheric soundings collected during the field campaigns. The Marine National Facility, the Australian Antarctic Division, the Atmospheric Radiation Measurement, and the National Science Foundation are referred to as MNF, AAD, ARM and NSF, respectively. The average number of soundings launched per day is denoted by "(avg)".

Campaign	Time period	Latitude range	Number of soundings (avg)	Time resolution (s)	Height resolution (m)	Type of sounding/ Platforms
SOCRATES	19/01/2018 – 24/02/2018	43°S – 62°S	109 (8)	0.5	5 – 6	Dropsondes/ The NCAR GV aircraft funded by the US NSF
CAPRICORN – 2016&2018	13/03/2016 – 13/04/2016	43°S – 54.5°S	31 (1)	2	8 – 12	Radiosondes/ The R/V Investigator funded by the MNF
	10/01/2018 – 21/02/2018	43°S – 65°S	235 (4)	1	3 – 5	Radiosondes/ The R/V Investigator funded by the MNF
MARCUS	19/10/2017– 23/03/2018	43°S – 69°S	460 (4)	2	8 – 12	Radiosondes/ The Aurora Australis funded by the ARM Facility
MICRE	01/04/2016 – 30/04/2018	54.61°S, 158.87°E	1351 (2)	2	8 – 12	Radiosondes/ Macquarie Island funded by the AAD and US ARM

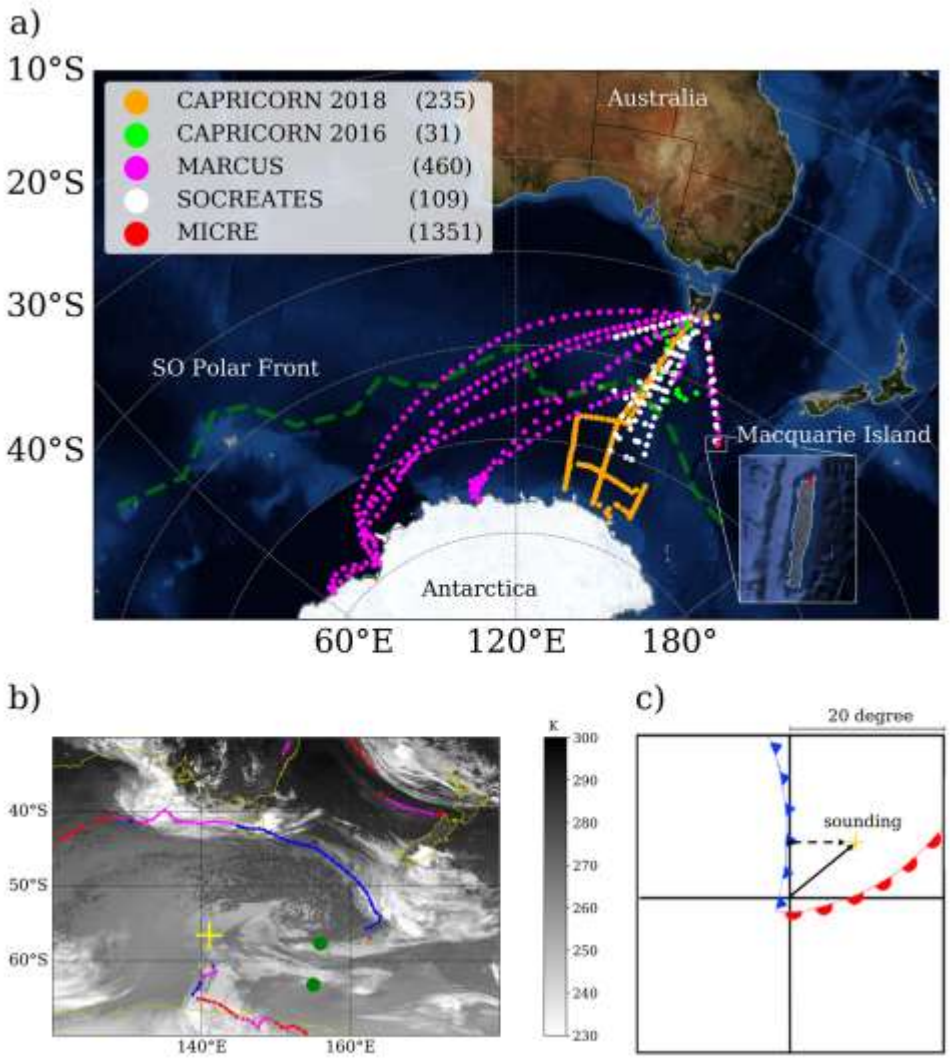

Figure 1. (a) The distribution of 2186 atmospheric soundings launched during the CAPRICORN 2016-2018, MARCUS, SOCRATES, and MICRE campaigns over the SO. The SO Polar Front is manually drawn from Dong et al. (2006). The Macquarie Island station is denoted by a red dot. (b) A snapshot of synoptic condition over the SO on 17 February 2018 at 19:00UTC showing the diagnosed cold, warm and stationary fronts as blue, red, and purple dotted lines, respectively. The diagnosed cyclone centres are represented as green dots. The shaded region is Himawari 8 brightness temperature (channel 13); with the sounding location is indicated as yellow plus label.

(c) Graphical illustration of the distances from a sounding to the nearest cyclone centre and the cold front, represented as the black solid and dashed lines, respectively.

Collectively these soundings do not represent a random sample across the SO; inherent spatial and/or temporal biases are present in each of the campaigns. For example, most of the campaigns were limited to the warm season months (November – April). Despite these limitations, the collection of soundings over the remote SO is unprecedented, especially at the higher latitudes poleward of the polar ocean front.

2.1 Cluster Identification

A simple *k*-means clustering algorithm (Anderberg 1973) is employed to sort these 2186 soundings according to their low-altitude thermodynamic structure, covering the MABL and the low-level cloud structure. The algorithm has been used extensively over the SO to study cloud regimes (e.g., Haynes et al., 2011; Mason et al., 2014), MABL in response to the synoptic forcing (e.g., Hande et al, 2012; L2018), only to cite a few. Following L2018, 4 variables (the temperature, relative humidity, zonal wind (u), and meridional wind (v)) at the 3 different levels of 925, 850, and 700 hPa and 3 surface variables (pressure, air temperature, and relative humidity) are used in the algorithm. Each variable is standardized ahead of clustering (i.e., zero mean and unit standard deviation). In this method, the number of clusters (denoted by k) have to be chosen as *a priori*. While our initial analysis was run with k ranging from 2 to 15 (not shown), k equal to 7 is chosen as it is the minimum number of clusters that effectively differentiates the synoptic environment of the studied region. The algorithm then iteratively partitions each aforementioned variable into the nearest cluster (equation (1)). Simple methods of clustering based only on the sea surface temperature (SST) or latitude where the soundings were launched were also undertaken but discarded, as these methods largely failed to reveal the influence of the varying synoptic meteorology, particularly across the SO storm track.

$$J = \sum_{j=1}^{k} \sum_{i=1}^{n} \left\| x_i^{(j)} - c_j \right\|^2, \qquad (1)$$

Where:

k	: number of cluster (k=7)
n	: number of soundings (n=2186)
$x_i^{(j)}$	: sounding i in cluster j
c_j	: centroid for cluster j
$x_i^{(j)} - c_j$	: Euclidean distance fuction

2.2 Cyclone Identification

The extratropical cyclones were detected using the Melbourne University cyclone detecting and tracking scheme (hereafter MU cyclone scheme; Murray and Simmonds 1991, Pezza et al., 2008). We used the mean sea level pressure (MSLP) obtained from the ERA5 reanalysis (Hersbach et al., 2020) with the time frequency of 3 hour and horizontal grid spacing of 0.25°. The algorithm maps the MSLP to a polar stereographic grid centred on the South Pole by bi-cubic spline interpolation, and then searches for the local maximum in the Laplacian of the MSLP field. Once the pressure minimum is identified, the cyclone is assigned as "open" or "closed" based on whether it has an open or closed isobar around the minimum. The cyclone

systems with its strength between 0.2 – 0.7 hPa (°lat)$^{-2}$ were classified as "weak" and those with the strength greater than 0.7 hPa (°lat)$^{-2}$ are as "strong". Detailed information of the MU cyclone scheme is given Lim and Simmonds (2007). In this work, we only used the closed cyclones, and focus on the instantaneous presence of the cyclones instead of their entire cyclone track. Grieger et al. (2018) compared results obtained with 14 schemes (including the MU cyclone scheme) over the higher latitudes of the SO and found significant agreement, particularly in the case of stronger cyclones, which suggests our results (Section 3) in connection with cyclone centres are robust. Each sounding was paired with the closest MU cyclone scheme centre within 20 degrees and within a 3-hour interval with the distance being calculated following L2018 (Fig. 1c).

2.3 Cold Front Identification

Cold fronts were identified with the objective front identification method developed by Hewson (1998) and improved by Berry et al. (2011). For this work, we used the specific humidity, temperature, *u* and *v* at the 850-hPa level obtained from the hourly ERA5 reanalysis at grid spacing of 0.75°. Locations of frontal points were identified where the horizontal gradient of the wet-bulb potential temperature following the moist isentropes at 850 hPa is a maximum. The diagnosed fronts were categorised into cold, warm, and quasi-stationary fronts as shown in Fig. 1b. As in the cyclone analysis, we analysed the diagnosed cold-front composite to better appreciate the influence of the cold front on the MABL structure, as similarly done in (Naud et al., 2016, 2015) and L2018. Following L2018, each sounding was paired with the closest diagnosed cold front within 15°, and the minimum distance in between was calculated. Sounding records were sorted by distance into 2.5° bins. The pre-/post-frontal (i.e., warm-/cold-air side) conditions are defined as positive/negative distances as in Fig.4. We note that previous authors (e.g. Schemm et al. 2014; Rudeva et al. 2019) have commented that this method is prone to identifying quasi-stationary fronts in coastal regions, such as the coast of Antarctica, where there are strong horizontal temperature/moisture gradients (see Fig. 3 of Berry at al. 2011).

2.4 Thermodynamic Metrics

Within the cluster and synoptic context, our analysis examines the physical characteristics of the atmospheric soundings, focussing on the low-level thermodynamic structure. Given that these various characteristics (e.g., inversion strength and height) are sensitive to the vertical resolution of the observations, all soundings have first been averaged onto a 20-m vertical grid, and then smoothed with a five-point running average as in L2018. This was necessary as the soundings were launched from an assortment of platforms (land-based and ship-based soundings and airborne dropsondes) featuring various spatial/temporal vertical resolutions (e.g. the dropsonde descent rate was greater than the weather balloon ascent rate).

2.4.1 Cloud Layers

Using only the thermodynamic sounding, we define a cloud layer as a layer with a dewpoint depression (i.e., the temperature and dewpoint temperature difference) of less than 1.5°C and a thickness of at least 60 m. For each upper-air sounding, the number of cloud layers from 500 m to 4000 m is counted. These thresholds were chosen to qualitatively reflect various field observations including a merged Radar-LiDAR product (Huang et al., 2019) from CAPRICORN 2016 and 2018 and airborne observations during SOCRATES. The results are not qualitatively sensitive to these thresholds.

We can define not only the number of individual cloud layers based on this definition, but also the total cloud geometric thickness. The cloud base height and cloud top height are defined as the altitudes of the cloud base of the lowest cloud layer and the cloud top of the highest cloud layer, respectively. Cloud layers are counted as no cloud, one layer, two layers and three+ layers. To be consistent with Mace et al. (2009), "multi-layer cloud" is counted if there are at least two layers identified in a sounding.

2.4.2 Inversion

There are numerous means of defining an inversion from radiosonde data (e.g., Zeng et al., 2004; Hande et al., 2012; L2018). In this work, the main inversion is identified as the level with maximum gradient of virtual potential temperature, $d\theta_v/dz$, from 500 to 4000 m above sea level with a minimum threshold of 0.14 Km^{-1}. If this threshold is not met between these heights, then 'no' inversion is recorded. Further inversions above this threshold are also counted. Note that these further inversions must be at least 300 m away from existing inversions. By this definition, we can simply count the number of inversions (i.e., $d\theta_v/dz \geq 0.14$ Km^{-1}) evident between 500 and 4000 m. A "multi-level inversion" is recorded if there are at least two inversions identified. The 0.14 Km^{-1} threshold is sensitive to the sounding vertical resolution, and was chosen upon visual inspection. Our findings are not qualitatively sensitive to small changes in this value.

The Lower Troposphere Stability (LTS; Klein & Hartmann, 1993) and Estimated Inversion Strength (EIS; Wood & Bretherton, 2006) are further investigated to understand the relationship between the low-altitude cloud amounts and lower-atmosphere stability over the SO. The LTS is calculated as the difference in the potential temperature between 700 hPa and the surface ($LTS = \theta_{700} - \theta_{surface}$). The EIS is defined as:

$$EIS = LTS - \Gamma_m^{850}(z_{700} - LCL), \qquad (2)$$

Γ_m^{850} is the moist adiabatic potential temperature gradient at 850 hPa; z_{700} is the altitude at 700 hPa level; and LCL is the lifting condensation level. A high EIS value relates to a strong and low-lying inversion which has been demonstrated to be a predictor of greater boundary layer cloud cover.

2.4.3 Boundary Layer Decoupling

Decoupling below the main inversion, as defined by Yin and Albrecht (2000), is also calculated. The parameter, μ, which measures the strength of the moisture and heat exchange at a transition layer (e.g., Yin and Albrecht 2000; Zhou et al., 2015; Mace and Protat 2018), is defined as:

$$\mu = -\left(\frac{\partial\theta}{\partial p} - \frac{0.608\theta}{1 + 0.608r}\frac{\partial r}{\partial p}\right), \qquad (3)$$

Where r, θ and p are the water vapour mixing ratio, potential temperature, and pressure respectively. Decoupling and a transition layer are defined when the ratio of the maximum positive value of μ is greater than 2.5 the average value. Both metrics, maximum μ and its average, are calculated from 500 m to the base of the main inversion.

3 Clustering Analysis

3.1 Geographical Distribution

The *k*-means cluster algorithm (*k*=7) was applied to the full collection of 2186 soundings. The clusters are then sorted by their mean SST for presentation purposes, only. We note that the SST, taken from the ERA5 reanalysis, is not employed in the clustering algorithm. The seven clusters are broadly separated into three main groups: one warm SST cluster (W1), four moderate SST clusters (M1, M2, M3, M4), and two cold SST clusters (C1, C2) (Fig. 2). The characteristics of these seven clusters are detailed in Table 2. The smallest cluster, C2, still contains 139 soundings, which suggests that the classification is solid and robust conclusions can be drawn.

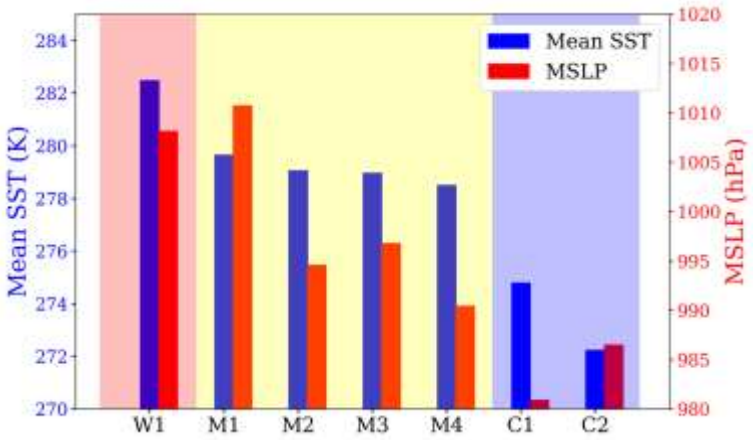

Figure 2. Bar plot of mean sea surface temperature (mean SST) and mean sea level pressure (MSLP) for the seven clusters from W1 to C2. The blue and red colour bars indicate the mean SST and MSLP, respectively. The shaded red, yellow, and blue regions represent the warm, moderate and cold SST clusters.

Soundings in the single warm SST cluster (W1) predominantly were those to the north of the ocean polar front while soundings in the two cold SST clusters reside predominantly poleward of the ocean polar front (Fig. 3a). The two cold SST clusters can be broken down further into soundings over the high latitudes of the SO (C1), in general, and those along the coast (C2). A sensitivity analysis confirmed that the composition of these two cold clusters was remarkably robust when the number of clusters was increased from 4 to 10 (not shown). Cluster C1 spans the region where polar mesocyclones are frequently observed (Carleton and Song 1997; Irving et al., 2010) and is host to very strong baroclinicity (Simmonds and Lim 2009). The soundings of the four moderate SST clusters span much of the domain between 40° and 60°S, but do not reach the coldest waters off the Antarctic coast. Further analysis reveals that these clusters capture various stages of the SO extratropical storms (Simmonds and Keay, 2000; Hoskins and Hodges, 2005), which will be discussed later.

Table 2. Cluster characteristics presented in terms of campaigns, seasonality, thermodynamic, cloud, inversion and microphysical properties. A number of soundings categorized by either campaign or seasonality are presented in sub-heading I and II, respectively. The notations of EIS, LTS and T_{air} stand for the Estimated Inversion Strength, the Lower Tropospheric Stability and the surface temperature, respectively. The wind speed, wind direction and relative humidity in sub-heading III are a mean value at 925 hPa.

Name of cluster	**W1**	**M1**	**M2**	**M3**	**M4**	**C1**	**C2**
I. Campaign							
SOCRATES	21	20	33	31	1	3	0
CAPRICORN 2016&2018	39	26	41	37	21	91	11
MARCUS	41	21	54	48	25	151	120
MICRE	108	205	379	291	287	73	8
Total count	209	272	507	407	334	318	139
II. Seasonality (MICRE only)							
Warm (Nov. – Apr.)	85	105	216	159	137	13	1
Cold (May – Oct.)	23	100	163	132	150	60	7
III. Thermodynamic							
SST (K)	282.5	279.6	279.1	279.0	278.5	274.8	272.2
SST – T_{air} (K)	-0.7	0.6	-0.3	1.6	-1.4	1.1	2.2
EIS (K)	10.05	9.43	5.53	4.5	7.27	6.38	8.86
LTS (K)	18.48	16.66	11.94	10.23	14.0	11.22	13.27
MSLP (hPa)	1008.1	1010.7	994.6	996.8	990.4	980.9	986.5
Wind speed ($m.s^{-1}$)	14.57	9.37	18.67	15.24	18.65	8.65	6.2
Wind direction (deg.)	294.9	268.8	282.6	242.8	331.2	126.6	99.0
Relative Humidity (%)	87.42	78.88	89.54	82.69	94.83	91.21	53.19
IV. Cloud Layer							
No cloud (%)	12.4	27.7	10.3	17.7	2.70	6.00	55.4
1 layer (%)	55.5	62.3	41.3	58.4	40.1	40.4	32.4
2 layer (%)	24.9	8.90	34.0	20.0	32.6	33.7	11.5
3+ layer (%)	7.20	1.10	12.6	3.90	17.4	16.4	0.70
Complete cloud (%)	0.00	0.00	1.80	0.00	7.20	3.50	0.00
V. Cloud Macro							
Total cloud thickness (m)	770±740	300±310	1080±920	560±520	1790±1090	1330±970	330±580
Cloud top height (m)	1910±1110	1280±830	2410±1090	1820±790	2890±1100	2540±1140	2610±1160
Cloud base height (m)	710±460	770±560	730±480	920±500	600±370	650±380	1610±940
VI. Inversion (INV)							
No INV (%)	10.5	11.0	35.3	22.6	52.1	37.7	15.1
1 INV (%)	39.7	33.2	33.2	34.7	30.3	38.8	28.0
2 INV (%)	27.8	32.9	20.0	28.9	16.4	16.7	32.4
3+ INV (%)	22.0	22.9	11.5	13.8	1.20	6.80	24.5
VII. INV Macro							
Main INV height (m)	1610±890	1570±870	2390±970	2270±860	2200±1070	2230±990	2170±870
Main INV strength ($K.m^{-1}$)	0.33±0.16	0.32±0.15	0.26±0.11	0.27±0.1	0.23±0.1	0.27±0.11	0.28±0.12
2^{nd} INV height (m)	2280±1000	2220±1010	2510±1000	2580±830	2360±1060	2290±1010	2410±940
2^{nd} INV strength ($K.m^{-1}$)	0.18±0.03	0.19±0.04	0.19±0.04	0.19±0.04	0.17±0.03	0.18±0.03	0.18±0.04

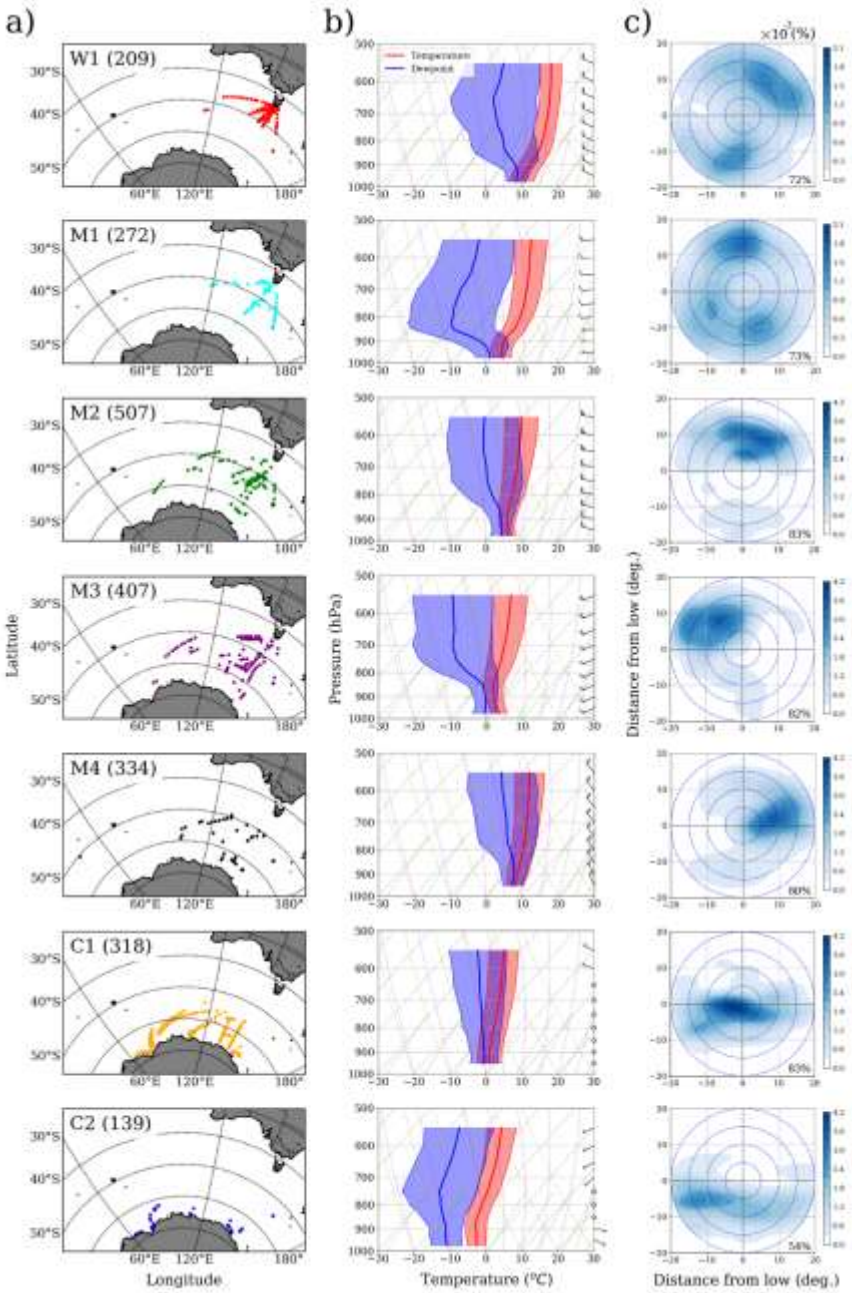

Figure 3. (a) Geographical distribution of soundings grouped by cluster for the seven clusters: W1, M1-M4, and C1-C2. (b) Mean profiles of temperature (red lines), dew point temperature (blue lines), and vector wind for the seven clusters as in (a), displayed as skew-T logP diagrams, shaded region indicating one standard deviation. (c) Frequency of occurrence composites of the sounding locations relative to the nearest cyclone centres for the seven clusters as in (a), circles denote the radius of 5°, 10°, 15° and 20° from the cyclone centre. The percentage (lower right) represents the number of soundings within 20° of the cyclone centre. A schematic of the location of the diagnosed cold and warm front in relation to the cyclone centre can be found in Fig. 1c.

Given that MICRE undertook soundings throughout the year, it is possible to look at the seasonality of the clusters at Macquarie Island. During the warm season (Nov – Apr) only 2% of the soundings belong to the cold clusters (C1 and C2), while 12% of the soundings belong to the warm cluster W1. During the cool season (May – Oct) 11% of the soundings belong to the two cold clusters, while 4% of the soundings belong to the warm cluster (Table 2). Macquarie Island resides to the north of the polar ocean front and is dominated by the soundings of the storm track clusters (M1-M4) throughout the year.

3.2 Thermodynamics Characteristics

A more comprehensive description of the seven clusters is obtained when the average MSLP and composite soundings are considered (Fig. 2 and Fig. 3b), particularly across the SO storm track. For example, warm cluster W1 has relatively strong winds from the northwest, suggesting that the airmass originated over warmer regions at lower latitudes. The composite sounding is relatively moist throughout the lowest levels and has a high mean MSLP of 1008.1 hPa (Table 2). The relatively high MSLP suggests that these soundings are, in general, far removed from any cyclonic low and/or are located at a lower latitude.

While the mean SST is insufficient to sort the four moderate clusters, their mean MSLP and wind speed and direction at 925 hPa help to differentiate them (Table 2). The mean MSLP ranges from 1010.7 hPa (M1) to 990.4 hPa (M4). We find that the model of a classic Norwegian front (Bjerknes and Solberg, 1922) is useful in describing these storm track clusters. The composite sounding of cluster M1 has weak westerly winds, high MSLP and a strong inversion at low elevation. We anticipate a significant coverage of stratocumulus clouds (closed mesoscale convective systems) at the top of the boundary layer as found by Muhlbauer et al. (2014). The composite M2 sounding has stronger westerly winds with a high humidity throughout the vertical profile. The MSLP drops, and the inversion increases in elevation and decreases in strength. The composite M3 sounding has slightly weaker winds from the southwest, the coldest surface temperature of the M clusters and a strong inversion around 850 hPa. The free troposphere is relatively dry above the inversion. Cluster M4, conversely, has strong northwesterly winds, a weak inversion and a high relative humidity throughout the vertical extent.

Turning to the two cold clusters, we note a sharp drop in mean MSLP, as these soundings ascents were made within the circumpolar trough (Simmonds and King 2004). Cluster C1 has the lowest mean MSLP at 980.9 hPa (Table 2). The composite profile also finds the weakest low-level wind speeds up to 650 hPa. Virtually no inversion is evident, and there is a high relative humidity up to 650 hPa. The final cluster, C2, is distinctly different from C1. C2 has a low relative humidity throughout, even in the surface layer. The composite suggests that many of these soundings were cloud free through 650 hPa. Approximately 35% of these soundings were

launched while the Aurora Australis was docked at Antarctic bases during the MARCUS campaign. We infer that C2 is influenced by strong katabatic outflows, which have frequently been reported along this part of the coast of Antarctica (e.g., Parish and Cassano, 2003; Bromwich et al., 2011). The C2 back trajectories in Figure 5 are illustrative. At higher resolution with topography (not shown) the lower two trajectories travel in and out of both sides of the valley which forms the drainage basin for the Amery Ice Shelf. We note that the katabatic wind typically extends to only less than 400-500 m above the surface.

3.3 Synoptic Classification

The broad influence of the synoptic meteorology on the thermodynamic structure of the boundary layer can be contextualized for each of the soundings using the MU cyclone composite analysis. The two-dimensional spatial density of the soundings (e.g. blue shaded regions in Fig. 3c) relative to the nearest cyclone centre is computed for each of the seven clusters (Fig. 3c). The mean latitude of the nearest cyclone centre shifts poleward (52.25°S – 60.14°S) and the mean MSLP drops (990.62 hPa – 973.30 hPa) when moving through the W to M to C clusters.

For warm cluster W1, there are only 3% of the soundings within 5° of the closest cyclone centre. Over 28% of the soundings are not within 20° of the nearest cyclone centre. The highest density is located in the northeast quadrant (Fig. 3c). Such a distribution pattern, together with the thermodynamic characteristics (Fig. 3b), suggests that W1 is generally present in the region far ahead of a cold front but after the ridging between fronts, where warm air from warmer water or the Australian continent is advected poleward. We note that W1 soundings can also be located in the southwest quadrant when a distant cut-off low over southwest Australia or the Tasman Sea is the closest cyclone centre.

Cluster M1 is similar to cluster W1 in that there is a relatively small percentage (13%) of soundings located within 10° of the nearest cyclone centre and a large percentage (over 27%) not within 20°. Coupled with the highest mean MSLP, M1 represents conditions associated with high-pressure systems and ridging, linked with large-scale subsidence. For cluster M2, however, the majority of the soundings are to the north-northeast of the cyclone centre with the peak density about 10° away. Coupled with the relatively low MSLP and the moist thermodynamic characteristics, these soundings are generalised as being near the cold front, but removed from the centre. Soundings in cluster M3 lie primarily to the northwest of the cyclone centre, consistent with the physical characteristics shown in the composite sounding, suggesting a relatively cold, post-frontal air mass. The greatest density of soundings in cluster M4 is immediately to the east of the cyclone centre. Given that M4 has the highest relative humidity of the four M clusters, this cluster is consistent with the warm front environment.

The greatest density of soundings for cluster C1 is located immediately to the south of the nearest cyclone centre. For cluster C2, the highest density of soundings is located just to the southwest of the cyclone centre. This westward displacement of this peak density is somewhat surprising, potentially reflecting a geographic bias in the generation of near coastal mesocyclones.

Turning to the distance to the nearest cold front (Fig. 4), the majority of soundings in cluster W1 are pre-frontal, which is consistent with a poleward transport of a relatively warm air mass. The distribution of the four M clusters relative to a cold front further supports our classic Norwegian fronts generalisation. Soundings from M1 (high pressure systems) are, in general, not

associated with any fronts. Soundings from M2 are frequently observed in the immediate neighbourhood of a cold front. Soundings in cluster M3 (post-frontal) are highly biased to post-frontal positions. Finally, the soundings in cluster M4 are, in general, ahead of the cold front, consistent with the location of the warm front. A more comprehensive analysis of the relationship between the Macquarie Island sounding and cold fronts over the SO is presented in L2018. While this methodology has been extended to higher latitudes, the findings are ambiguous presumably due to difficulties in resolving cold fronts associated with polar mesocyclones (Berry et al., 2011).

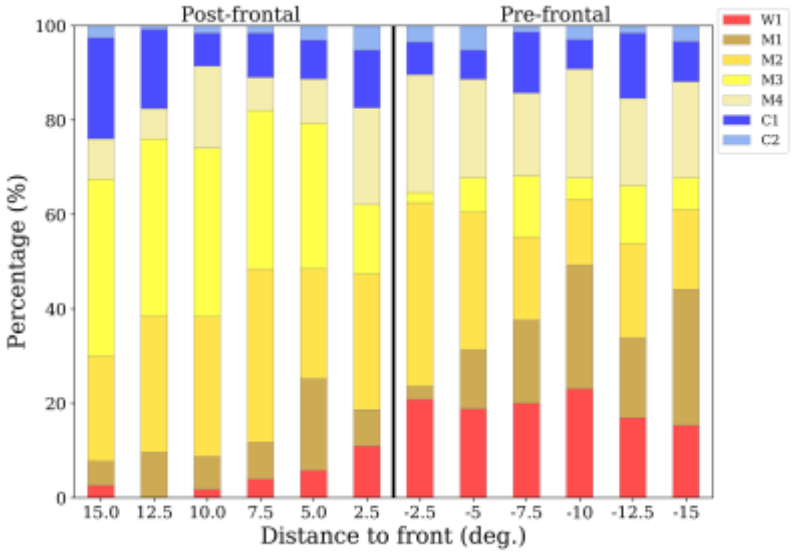

Figure 4. Stacked bar plot grouped by 2.5° bins showing the distance from the sounding to a cold front for the seven clusters: W1, M1-M4, and C1-C2.

The associated character of the surface forcing (SST – surface air temperature; Table 2) further supports the model of the Norwegian front. A positive (negative) difference in the surface forcing corresponds to cold (warm) air advection. Clusters W1 and M4 display strong warm air advection, while cluster M2 displays strong cold air advection. Notably, the strongest cold air advection is off the coast of Antarctica in cluster C2. The soundings in cluster C1 also display cold air advection suggesting the surface layer is unstable through the high latitudes of the SO.

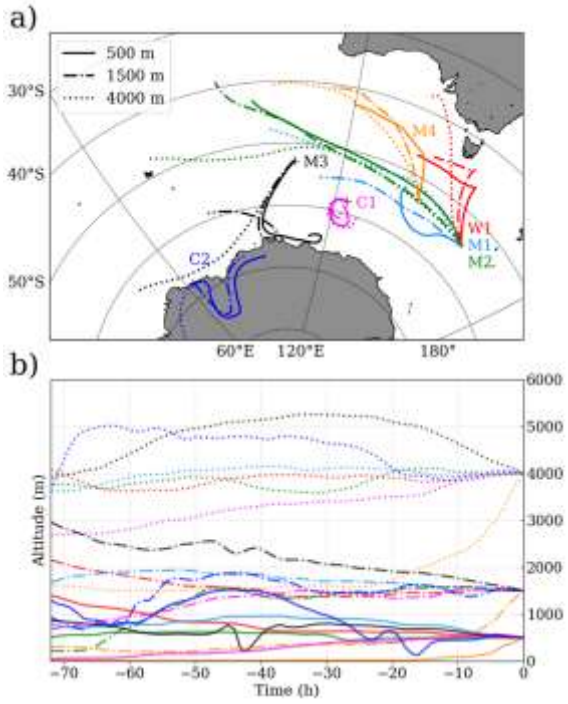

Figure 5. (a) 72-h HYSPLIT back trajectory for the nearest soundings to the centroid in each cluster: W1, M1-M4, and C1-C2, separately. The back trajectories were calculated using Global Data Assimilation System meteorological data at 1° horizontal resolution. The solid, dash-dotted, and dotted lines represent the vertical tracks from 500, 1500, and 4000 m above ground level, respectively. (b) Vertical back trajectories for each cluster with colour corresponding to the tracks as in (a).

Fig. 5 shows a single 72-hour multi-level back trajectory of a typical air mass of each cluster, calculated with the HYbrid Single Particle Lagrangian Integrated Trajectory Model (HYSPLIT, Stein et al., 2015). For example, the back trajectories of C1 is consistent with cyclonic flow around a low. The back trajectories of M3 is of interest since the lower and upper level wind were easterly and westerly, respectively, prior to change to the southwest before arriving at the sounding location. Further analysis (not shown) indicates that the presence of low pressure polar mesocyclones along the coast of Antarctica in the vicinity of the back trajectories can potentially cause the observed discrepancies. Generally, the seven back trajectories as shown in Fig. 5a are consistent and further illustrate our interpretation of the synoptic nature of each cluster as discussed in the section 3.1 and 3.2.

In summary, seven distinct clusters have been identified that capture the influence of the synoptic meteorology on the low-level thermodynamic structure over the SO.

- Cluster W1 typically captures poleward warm air advection far ahead of a cold front. While some of these soundings located as far south as Macquarie Island, none is observed to be poleward of the ocean polar front.
- Cluster M1, the high-pressure cluster, is characterized by weak winds, a strong inversion and low relative humidity in the free troposphere.
- The remaining moderate SST clusters capture the different sectors of mid-latitude cyclones over the SO: M2 – the cold front cluster, M3 – the post-frontal cluster, and M4 – the warm front cluster. Soundings in these clusters generally have strong westerly winds.
- Cluster C1, the high-latitude SO cluster, is predominantly located poleward of the ocean polar front with weak winds through the boundary layer and high relatively humidity through the lower free troposphere.
- Cluster C2, the Antarctic coastline cluster, commonly displays dry off-shore flow, consistent with katabatic winds across the lowest 200 to 500 meters.

It should be noted that the labelling is only used to provide generality in the mean behaviours of the clusters – it should not be interpreted as the absolute nature of the individual soundings.

4 Cloud layers, Inversions and Decoupling

In this section we present a statistical analysis of multi-layer cloud, multi-level inversion and decoupling for each cluster, to provide further understanding of key thermodynamic parameters in the SO MABL.

4.1 Cloud Layers

One of our primary interests is to better appreciate the thermodynamic structure of the "multi-layer" clouds reported in Mace et al. (2009) in the high latitudes of the SO. To assist in this we consider the number of cloud layers (no cloud, 1-layer, 2-layer, 3+layer and solid cloud) between 500 and 4000 m, as well as the total cloud thickness, uppermost cloud top and lowermost cloud bottom heights between these altitudes (Table 2).

Starting again with the warm cluster, W1, a single cloud layer is most frequently observed (55.5%), followed by two layers (24.9%). The high-pressure cluster, M1, commonly has one (62.3%) or no (27.7%) cloud layers. On average, M1 has a relatively thin amount of cloud (300 m) and the lowest cloud-top height (1280 m). Not surprisingly, clouds under these conditions most closely resemble those found in sub-tropical maritime subsidence regions. The cold front cluster, M2, has few no cloud layers (only 10.3%) soundings and more multi-cloud layers. The thickness of clouds through these soundings has increased (1080 m) as has the uppermost cloud-top height (2410 m). The post-frontal cluster, M3, generally has one cloud layer (58.4%). The lowermost cloud base height for these soundings rises to an average of 920 m. Ahn et al. (2017) commonly observed open mesoscale cellular convection in such conditions. The warm front cluster, M4, has the lowest frequency of no cloud layers (2.7%) and a large frequency of multi-layer cloud soundings (50%), suggesting a complex vertical structure. Solid cloud deck from 500 m to 4000 m are most commonly observed (7.2%) in this cluster. The average total cloud thickness is 1790 m, and the average uppermost cloud-top height is 2890 m.

Turning to the high-latitude SO cluster, C1, our results are consistent with Mace et al. (2009). The largest frequency of multi-layer cloud soundings occurs over these cold waters (50.1%). The average accumulated cloud thickness is 1330 m and the uppermost cloud-top height is at 2540 m. Consistent with the A-train satellite observations of Huang et al. (2015), the cloud-top height is greater over the high latitudes than along the storm track (average of M1-M4). The cloud macrophysics change dramatically when moving from C1 to C2. Along the Antarctic coast cloud-free conditions are observed 55.4% of the time, consistent with the composite sounding (Fig. 3b). When clouds are present, they are predominantly found as a relatively thin, single layer. The average lowermost cloud base for C2 is at a relatively high altitude (1610 m).

4.2 Inversions

Past field observations over the SO have often revealed a complex boundary layer structure with multiple inversions and strong wind shear (e.g., Russell et al. 1998; Jensen et al. 2000). Building on our cluster framework, we extend our analysis to consider the nature of inversions from 500 – 4000 m. Soundings within the warm cluster, W1, generally have one (39.7%) or two (27.8%) inversions. The primary inversion is at a relatively low altitude (1610 m) and is strong (0.33 K m^{-1}). The inversion structure in cluster M1 (high pressure) is similar, the primary inversion is again relatively low (1570 m) and strong (0.32 K m^{-1}), as we would expect in a region of strong subsidence. For both of these clusters, when a secondary inversion is observed, it is commonly found above the primary inversion around 2200 m, which is distinctly different than over subtropical regions. For both of these clusters, it is also relatively common to find three or more inversions (22%), again markedly different than over the subtropics.

Turning to clusters M2, M3 and M4, the average altitude of the main inversion increases to over 2200 m, and the strength of the inversion decreases, which is consistent as low-level subsidence is giving way to low-level convergence/instability generated by cyclone dynamics. Compared to W1 and M1, it is far more common to observe no clear inversion through the lower free troposphere, especially in the warm front cluster, M4 (52.1%). Multiple inversions are less common compared to clusters W1 and M1. The average height of a secondary inversion, if present, is only slightly greater than that of the primary inversion, suggesting that it can be on either side of the primary inversion.

The inversion structure for cluster C1 is very similar to that of M4. Both of these clusters are associated with low MSLP suggesting low-level convergence and convection. In this region, where it is frequent to observe multiple cloud layers, it is rare to observe multiple inversions (23.5%), suggesting that these cloud layers can reside at weak inversions below the threshold within weak static stability. Beyond convective turbulence, the relatively weak wind speeds of C1 soundings may allow any inversion to be further eroded through radiation.

Finally looking at the Antarctic coastline cluster, C2, we see the greatest frequency of multiple inversions (55.9%), but often without cloud as discussed previously. The secondary inversion is, on average, located above the primary inversion. The common presence of dry, multi-level inversions near the Antarctic coastline suggests that the thermodynamic structure of the air mass can be influenced by dry, descending katabatic outflows, interacting with large-scale horizontal advection. These persistent katabatic winds over the Antarctic continental margins have been found to be a key component in supplying the lower troposphere with unsaturated air (Grazioli et al., 2017).

For all seven clusters, the mean height of the secondary inversion – when present – is greater than the mean height of the primary inversion, even under strong subsidence (clusters W1 and M1). The physical significance of this relationship is ambiguous, given that there are fewer soundings with multiple inversions. Similarly, we note that cloud layers are often not collocated with inversions. The two case studies will demonstrate these relationships.

Finally, we examine LTS and EIS across the clusters (equation (2)). Observations from a collection of MABL field campaigns have established a simple linear relationship between these metrics and the low-level fractional cloud cover. These authors note, however, that these metrics are appropriate in a suppressed environment. Consistent with this constraint, we find that the warm cluster (W1) and the high-pressure cluster (M1) have a relatively high LTS/EIS and fractional cloud cover (1 – "no cloud" frequency) that reasonably fit the linear relationships of Wood and Bretheron (2006). These two clusters have more subsidence/suppressed conditions. The remaining five clusters, however, are poorly served by this relationship.

4.3 Decoupling

Our cluster analysis suggests that the LLWAA scenario (Zheng and Li 2019) should most likely occur in cluster W1 and M4, where warm air routinely travels poleward via north-westerly winds in the lower troposphere (Fig. 3b and Table 2). Indeed, 25 of the 26 soundings examined in Zheng and Li (2019) fall into cluster W1. Given that soundings in clusters W1 and M4 are most frequently present over the low-/mid- latitudes of the SO and/or in the warm sector of the cyclones, these clusters are unlikely to play a key role in explaining the model errors most pronounced at the high-latitude SO and the frequent occurrence of multi-layer clouds.

Overall, we found that a simple MABL structure (where no cloud or secondary inversion was identified above the main inversion) existed for 55% of the 2186 soundings. We further evaluated these simple MABL soundings to futher investigate the presence of decoupling based on the parameter μ (equation (3)); only 38% of these soundings qualified as being decoupled. This means that, regardless of the underlying mechanisms, only 20% of all 2186 soundings were characterised as a simple decoupled MABL. Such soundings were most common in cluster M3 (33%) and least common in cluster C1 (12%). While this simple calculation has neglected the possibility that a decoupled MABL may exist within a complex multi-layer structure, it demonstrates the necessity to go beyond the MABL to fully understand the thermodynamic and cloud processes over the high-latitude SO. In that regard, these decoupling mechanisms are inadequate to describe key physical processes, where multi-layer clouds are prevalent over the SO.We further note that our lower altitude boundary (500 m) is likely to preclude the analysis of any surface layer inversion.

Through the lower troposphere the cloud structure (i.e. number of layers and overall thickness) and inversion structure (i.e. strength, height and 'decoupling') vary by cluster.

- A multi-layer cloud structure is frequently found in the cold front cluster (M2), the warm front cluster (M4) and the high-latitude cluster (C1) where there is a high relative humidity above the boundary layer.
- The main inversion tends to be at a lower elevation and stronger over the low-latitudes (clusters W1 and M1), but tends to be higher and weaker in the mid- and high-latitude. Further, the EIS and LTS metrics are skillful in estimating the low level cloud cover in these two low-latitude clusters, where the MSLP is relatively

high. On the contrary, these measures are less skillful for the mid- and high-latitude clusters.

- A 'decoupled' boundary layer is found to be infrequent over the mid- and high-latitude. A simple decoupled boundary layer was observed most commonly (~33%) in the post-frontal cluster, M3, where the clouds are largely confined to the boundary layer.
- Clusters with multiple cloud layers (C1 and M4) are associated with weak inversions, even below the defined threshold. Under these conditions, there's little connection between cloud layers and the elevation of inversions.

5 Case Studies

The bias in shortwave radiation over the SO is commonly depicted at the high latitudes (cluster C1) and behind cold fronts (cluster M3) (e.g. Bodas-Salcedo et al. 2012; Williams et al. 2013). Yet these two clusters differ in numerous respects including cloud layers, inversion strength, relative humidity and wind speed. Representative case studies are presented for both clusters as a means to explore key dynamical and physical processes and the relationship to the synoptic meteorology. Unfortunately, space limitations precludes an analysis of all seven clusters.

5.1 Post-frontal Environment (M3)

On 17 February 2018, the RV Investigator had an eastward heading, sampling from 134.6°E to 142.2°E at 56.57°S. The MSLP at 00:00UTC 18 February 2018 (Fig. 6a) shows the closest low-pressure system present near 160°E, 60°S. A high-pressure system was located over the Great Australian Bight at 130°E, 45°S, ridging southward. The MSLP suggests relatively strong south-westerly winds at the surface in a post-frontal environment, consistent with our description of cluster M3. Fig. 6(b) displays the location of the ship (yellow plus symbol) and diagnosed fronts and cyclone centres overlaying the shaded Himawari-8 brightness temperature (channel 13). Note that the nearest cyclone identified by the MU cyclone scheme was located near 155.9°E, 57.7°S at this time.

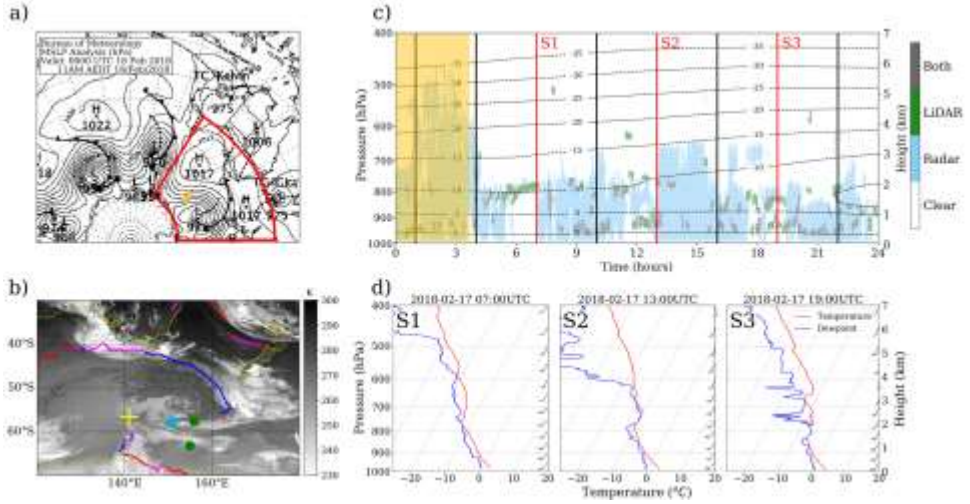

Figure 6. (a) MSLP analysis provided by the Bureau of Meteorology, Melbourne, Australia at 00:00UTC 18 February 2018. '11AM EST' indicates Australian Eastern Standard Time, 11 h ahead of UTC. Red box indicates the domain of interest as shown in (b). (b) As presented in Fig. 1b except for the diagnosed cyclone centre in question is indicated in skyblue dot. (c) The cloud mask product including Clear, Radar, LiDAR, and Both presented as white, skyblue, green, and grey colour shaded regions, respectively. The dashed line is the temperature derived from ERA-Interim. The vertical lines are the sounding launched times. The orange shaded region indicates the first sounding of the date, which is belong to C1, not M3. (d) Three typical soundings launched during the day at 07:00, 13:00, 19:00UTC 17 February 2018, corresponding to the vertical red lines in (c).

Fig. 6(c) shows the time series of cloud cover type vertical profiles from a merged cloud Radar-LiDAR product (Huang et al. 2019) for the duration of 19 hours (05:00 – 23:59UTC). Most of the clouds were observed to reside in the lowest 3.5 km during this period. While thicker clouds were observed to be precipitating intermittently, multi-layer thin clouds were also frequently detected. Most of these multi-layer clouds were non-precipitating, with their primary cloud-top varying between 2 and 3.5 km altitude.

There were six soundings launched from the ship during the 19 hours, all of which were classified as cluster M3. Fig. 6(d) shows the three soundings launched at 07:00, 13:00, 19:00UTC, all of which display multiple layers of saturation, consistent with the multi-layer clouds shown in the cloud-type product. Note that the saturation layers (observed in soundings) and cloud layers (detected by Radar-LiDAR) are not expected to be perfectly collocated, given the rapid drifting of the radiosondes. Looking at sounding S3 at 19:00UTC 17 February 2018, there are four layers of near saturation where a cloud could potentially be present (thin layers at 920, 870 and 680 hPa and a thicker region from 830-780 hPa), although the merged cloud mask does not detect any cloud at 680 hPa at this time. In addition, while our metrics identified four cloud layers (with a total cloud thickness of 1620 m), only three inversions were identified with

the main inversion at 653 hPa. Only the cloud layer and inversion at approximately 775 hPa are collocated. Similar structural variability is also present in sounding S1 and S2.

Commonly residing in the post-frontal air mass, M3 cluster typically has strong cold air advection in the lower troposphere (Table 2). The multi-layer structure and moist free troposphere does not, however, resemble the subtropics. There is no evidence of substantial convection immediately near these soundings, suggesting that the source of moisture at the upper levels needs to be from horizontal advection. A closer examination on the Himawari-8 image and back trajectories (not shown) suggests that the upper level moisture may have originated in the frontal cloud band located south of the ship.

5.2 High-latitude Southern Ocean (C1)

The MSLP at 00:00UTC 16 February 2018 (Fig. 7a) shows several polar mesocyclones near Antarctica. The ship was located near a cyclone centre at 132.0°E, 57.51°S, about 15° away from the Antarctic coast. Throughout the day, the relative position of the ship changed from being in the south-eastern side to the south-western side of the nearest cyclone centre (Fig. 7b).

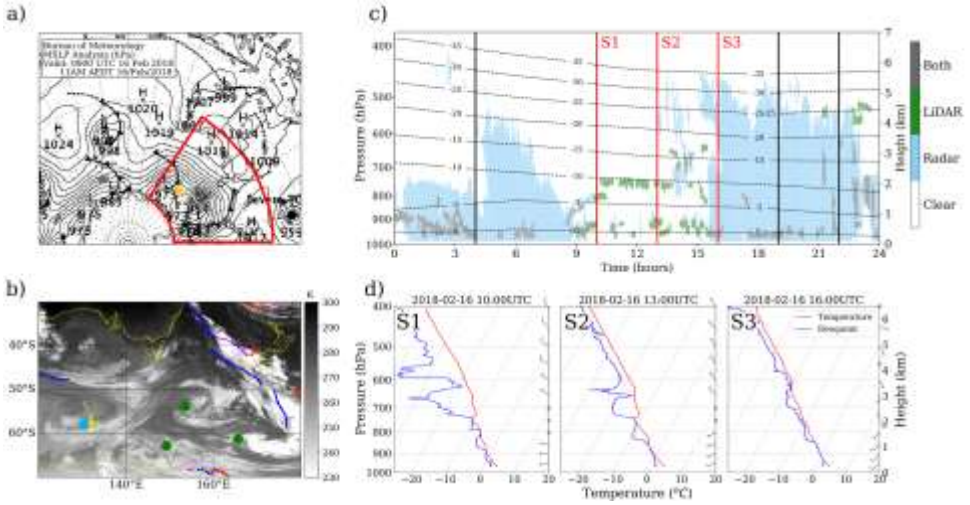

Figure 7. (a) As for Fig. 6(a) but at 00:00UTC 16 February 2018. (b) As for Fig. 6(b) but at 16 February 2018 at 10:00UTC. (c) As for Fig. 6(c) except for the shaded region. (d) Three typical soundings launched during the day at 10:00, 13:00, and 16:00UTC 16 February 2018.

The time series of the cloud cover type shows that multi-layer thin clouds, most of which resided in the lowest 3.5 km, were detected from 09:00 to 16:00UTC (Fig. 7c). The cloud field was characterized by scattered stratus and cumulus in the lowest kilometer, likely resulting from cold air advection, and a more extensive cloud layer present at 2 km. Thicker precipitating clouds were again commonly detected up to 5 km, reflecting the moist lower troposphere near the cyclone centre. Unlike the classic structure of mid-latitude cyclones where cirrostratus abound near and around the cyclone centre (e.g., Field and Wood 2007), such thick high clouds were rarely detected in this case as the ship progressed through the mesocyclone.

Six soundings were launched throughout the day, all of which were in cluster C1. In three consecutive soundings, various stages of the multi-layer cloud cover were captured (Fig. 7d). The sounding at 16 February 2018 (Fig. 7d, S1) detected four layers of saturation where cloud could potentially be present (thin layers at 930, 880, 790 and 740 hPa), although only three cloud layers are visible in the Radar-LiDAR observation at this time. The single main inversion was identified at 733.1 hPa with a strength of 0.2 K m^{-1}, collocated with the cloud layer at that level. It is interesting to note the weak local wind speed with shifting wind direction, reflective of the wind flow ringing the mesocyclone. The following two sounding profiles exhibit a similar vertical structure, despite the slight moistening of the mid-troposphere towards the later time of the day.

Unlike the M3 case study, the persistent multi-layer mid-top clouds in this case were produced in a dynamically evolving environment around a cyclone centre, where high-top thick clouds were typically expected. As such, the layer clouds in the mid-troposphere could readily be altostratus and/or altocumulus shelf clouds detraining from active convection in the vicinity of the mesocyclone centre.

6 Discussion and Conclusion

In this study, we have utilized 2186 high-resolution soundings from four recent field campaigns to construct a climatology of the marine atmospheric boundary layer (MABL) and the lower free troposphere over the Southern Ocean (SO) using a *k*-means cluster analysis. Relationships between the thermodynamic structure and the synoptic meteorology have been examined using fronts and cyclone composite analyses. In addition to documenting the statistics of a set of thermodynamic parameters including cloud and inversion measures, we have also examined features unique to the high-latitude SO region, such as the presence of multiple cloud layers and multiple inversion layers.

We found that the low-level thermodynamic structure can be classified into seven distinct clusters. A warm cluster, W1, typically depicts the warm air advection far ahead of a cold front. The high-pressure cluster, M1, represents large-scale subsidence with a strong inversion and low relative humidity in the free troposphere. The three clusters M2, M3 and M4 generally correspond to the classic Norwegian front theory. Specifically, the cold front cluster, M2, describes an environment being near the cold front, but removed from the cyclone centre. The post-frontal cluster, M3, often resides in the northwest of the cyclone centre. The warm front cluster, M4, is positioned in the northeast of the cyclone centre. C1 is generally located poleward of the ocean polar front and in vicinity of the cyclone centre. C2 is characterized by a dry and cold atmosphere, generally cloud free, typically found along the Antarctic coastline. Overall, the general characteristics of the clusters W1 and M1-M4 and their response to the synoptic forcing are consistent with the findings in L2018 using 16-year soundings from Macquarie Island. The two new clusters C1 and C2 identified in this study are uniquely present only over the high-latitude SO.

We further investigated the number of cloud layers by conducting a simple cloud count between 500 m and 4000 m. The results reveal some level of dependency on the synoptic meteorology. One-layer cloud is most prevalent in the warm cluster (W1), the high-pressure cluster (M1) and the post-frontal cluster (M3), presenting 55.5%, 62.3% and 58.4% of the time, respectively. A multi-layer cloud structure is more common in the cold front cluster M2 (46.6%),

the warm front cluster M4 (50.0%), and the high-latitude SO cluster C1 (50.1%). In the Antarctic coastline cluster, C2, cloud-free conditions are observed 55.4% of the time.

A similar analysis on the nature of the inversion structure has also been carried out. In clusters W1 and M1 with strong MSLP, the primary inversion is commonly found to be strong (0.32 $K.m^{-1}$) and at low altitudes (1570 m). Two or more inversions are still relatively common in these two clusters. In clusters M2, M3, M4 and C1, the main inversion tends to be higher and weaker, while a multi-level inversion structure is relatively infrequent. The Antarctic coastline cluster, C2, has the highest frequency of multiple inversions (55.9%). The Estimated Inversion Strength (EIS) and Lower Tropospheric Stability (LTS) were found to be skilled in estimating the low-altitude fractional cloud cover in the two clusters with relatively high mean sea level pressure (W1 and M1). Conversely, these relationships failed for clusters associated with the SO storm track (M2, M3 & M4) and higher latitudes (C1 and C2).

Overall, our findings suggest that multiple cloud layers and inversions are fairly common over the SO, consistent with the previous satellite-based climatology of Mace et al. (2009) and earlier studies using limited observations from past field campaigns (e.g., Russell et al. 1998; Jensen et al. 2000). Building on this, our analysis provides further details on the thermodynamic structures in relation to synoptic forcing and environmental conditions, casting new light on the basic dynamics and physical processes.

Although a decoupled boundary layer has been reported to be common over the SO in recent studies (e.g., Zheng and Li 2019; Mace and Protat 2018), our analysis suggests that only 20% of the 2186 soundings can readily be characterised as a simple, decoupled boundary layer under a homogenous free troposphere. Such soundings are most frequently found in cluster M3 (33%) and least frequently in cluster C1 (12%). Similarly, decoupling induced by LLWAA as reported in Zheng and Li (2019) is most likely to happen in cluster W1 and potentially in M4. As such, these decoupling mechanisms are insufficient in explaining key processes over the high-latitude SO, where multi-layer clouds abound.

Our preliminary examinations of the multi-layer systems suggest that the source of moisture at the upper levels tends to be aloft and not at or near the surface. As such, we expect that cold/warm air advection on the upper levels and detrainment of convection associated with high-latitude mesocyclones are potential drivers of the multi-layer clouds over the SO. If this is true, then the LLWAA decoupling seems to be a misnomer since the different layers were never initially a single well-mixed layer. In future work, we will use more comprehensive field data in conjunction with numerical simulations to investigate the detailed processes.

Given the importance of how the cloud vertical structure is represented in climate models to the calculation of the radiative properties, knowledge of cloud vertical structure will provide critical information for understanding the radiation biases in climate models, which is significant over the high-latitude SO. Such knowledge is also paramount for characterizing the vertical distribution of latent heat release that could affect large-scale circulations and precipitation. As such, the observational analysis in this study has shed light on fundamental issues such as the radiation bias facing the climate modelling community today.

Acknowledgments

This work is supported by an Australian Research Council discovery grant DP190101362. The authors deeply thank the entire CAPRICORN, MARCUS, MICRE and

SOCRATES teams for their tremendous efforts and dedication in collecting the datasets. We thank the CSIRO MNF for its great support and service. We greatly appreciate Micheal Reeder from Monash University for providing support with the front identification algorithm. All data are currently available at the Earth Observing Laboratory website (https://data.eol.ucar.edu/master_lists/generated/socrates/). We sincerely thank Alain Protat at The Bureau of Meteorology, Australia and Dr. Peter May at Monash University for insightful comments on the work.

References

Anderberg, M. R. (1973), Cluster analysis for applications. Monographs and textbooks on probability and mathematical statistics. New York: *Academic Press*

Ahn, E., Huang, Y., Chubb, T. H., Baumgardner, D., Isaac, P., de Hoog, M., et al. (2017), In situ observations of wintertime low-altitude clouds over the Southern Ocean. *Quarterly Journal of the Royal Meteorological Society*, 143(704), 1381–1394. https://doi.org/10.1002/qj.3011

Albrecht, B. A., C. S. Bretherton, D. Johnson, W. H. Scubert, and A. S. Frisch, (1995), The Atlantic Stratocumulus Transition Experiment-ASTEX. *Bulletin of the American Meteorological Society*, 76, 889–904, https://doi:10.1175/1520-0477(1995)076,0889:TASTE.2.0.CO;2

Berry, G., Reeder, M. J., & Jakob, C. (2011), A global climatology of atmospheric fronts. *Geophysical Research Letters*, 38, L04809. https://doi.org/10.1029/2010GL046451

Bjerknes, J., and H. Solberg (1922), Life cycle of cyclones and the polar front theory of atmospheric circulation, *Geophysisks Publikationer*, 3, 1–18

Bodas-Salcedo, A., Williams, K. D., Field, P. R., & Lock, A. P. (2012), The surface downwelling solar radiation surplus over the Southern Ocean in the Met Office model: The role of midlatitude cyclone clouds. *Journal Climate*, 25(21), 7467–7486. https://doi.org/10.1175/JCLI-D-11-00702.1

Bretherton, C. S., and M. C. Wyant, (1997), Moisture transport, lower-tropospheric stability, and decoupling of cloud-topped boundary layers. *Journal of the Atmospheric Sciences*, 54, 148–167, https://doi:10.1175/1520-0469(1997)054,0148: MTLTSA.2.0.CO;2

Bromwich, D. H., D. F. Steinhoff, I. Simmonds, K. Keay, and R. L. Fogt (2011), Climatological aspects of cyclogenesis near Adélie Land Antarctica, *Tellus A: Dynamic Meteorology and Oceanography*, 63A, 921–938, doi: 10.1111/j.1600-0870.2011.00537.x

Carleton, A. M., and Y. D. Song, (1997), Synoptic climatology and intrahemispheric associations of cold air mesocyclones in the Australasian sector. *Journal of Geophysical Research: Atmospheres*, 102, 13 873–13 887. https://doi.org/10.1029/96JD03357

Dong, S., Sprintall, J., & Gille, S.T. (2006), Location of the Antarctic polar front from AMSR-E satellite sea surface temperature measurements. *Journal of Physical Oceanography*, 36(11), 2075–2089. https://doi.org/10.1175/JPO2973.1

Christensen, M. W., Carrió, G. G., Stephens, G. L., and Cotton, R., (2013), Radiative impacts of free-tropospheric clouds on the properties of marine stratocumulus, *Journal of the Atmospheric Sciences*, 70, 3102–3118, 2013. https://doi.org/10.1175/JAS-D-12-0287.1

Field, P. R., and R. Wood, (2007), Precipitation and cloud structure in midlatitude cyclones. *Journal Climate*, 20, 233–254, https:// doi.org/10.1175/JCLI3998.1

Furtado, K., and P. Field, (2017), The role of ice microphysics parametrizations in determining the prevalence of supercooled liquid water in high-resolution simulations of a Southern Ocean midlatitude cyclone. *Journal of the Atmospheric Sciences*, 74, 2001–2021, https://doi.org/10.1175/JAS-D-16-0165.1

Grazioli, J., Madeleine, J.-B., Gallée, H., Forbes, R. M., Genthon, C., Krinner, G., and Berne, A. (2017), Katabatic winds diminish precipitation contribution to the Antarctic ice mass balance, *Proceedings of the National Academy of Sciences of the United States of America*, 114, 10858–10863, https://doi.org/10.1073/pnas.1707633114

Grieger, J., G. C. Leckebusch, C. C. Raible, I. Rudeva, and I. Simmonds (2018), Subantarctic cyclones identified by 14 tracking methods, and their role for moisture transports into the continent, *Tellus A: Dynamic Meteorology and Oceanography*, 70A, 1454808, doi: 10.1080/16000870.2018.1454808

Hande, L. B., Siems, S. T., Manton, M. J., & Belusic, D. (2012), Observations of wind shear over the Southern Ocean. *Journal of Geophysical Research: Atmospheres*, 117, D12206. https://doi.org/10.1029/2012JD017488

Haynes, C. Jakob, W. B. Rossow, G. Tselioudis, and J. Brown, (2011), Major characteristics of Southern Ocean cloud regimes and their effects on the energy budget. *Journal Climate*, 24, 5061–5080. https://doi.org/10.1175/2011JCLI4052.1

Hersbach H, Bell B, Berrisford P, et al. The ERA5 global reanalysis. *Quarterly Journal of the Royal Meteorological Society*. 2020;1–51. https://doi.org/10.1002/qj.3803

Hewson, T.D. (1998), Objective fronts. *Meteorological Applications*, 5(1), 37–65. https://doi.org/10.1017/S1350482798000553

Hoskins, B. J., & Hodges, K. I. (2005), A new perspective on Southern Hemisphere storm tracks. *Journal Climate*, 18(20), 4108–4129. https://doi.org/10.1175/JCLI3570.1

Huang, Y., M. Manton, S. Siems, A. Protat, L. Majewskic, and H. Nguyen (2019), Evaluating Himawari-8 Cloud Products Using Shipborne and CALIPSO Observations: Cloud-top Height and Cloud-top Temperature. *Journal of Atmospheric and Oceanic Technology*, 36, 2327-2347, DOI: 10.1175/JTECH-D-18-0231.1

Huang, Y., Protat, A., Siems, S. T., & Manton, M. J. (2015), A-train observations of maritime midlatitude storm-track cloud systems: comparing the Southern Ocean against the North Atlantic. *Journal Climate*, 28(5), 1920–1939. https://doi.org/10.1175/JCLI-D-14-00169.1

Huang, Y., Siems, S. T., Manton, M. J., & Thompson, G. (2014), An evaluation of WRF simulations of clouds over the Southern Ocean with A-Train observations. *Monthly Weather Review*, 142(2), 647–667. https://doi.org/10.1175/MWR-D-13-00128.1

Huang, Y., Siems, S. T., Manton, M. J., Hande, L. B., & Haynes, J. M. (2012a), The structure of low-altitude clouds over the Southern Ocean as seen by CloudSat. *Journal Climate*, 25(7), 2535–2546. https://doi.org/10.1175/JCLI-D-11-00131.1

Huang, Y., Siems, S. T., Manton, M. J., Hande, L. B., & Delanoë , J.. (2012b), A study on the low- altitude clouds over the Southern Ocean using the DARDAR- MASK. *Journal of*

Geophysical Research: Atmospheres, 117, D18204, https://doi.org/10.1029/2012JD017800

Hyder, P. et al., 2018, Critical Southern Ocean climate model biases traced to atmospheric model cloud errors. *Nature Communications*, 9, 3625, doi: 10.1038/s41467-018-05634-2

Irving, D., I. Simmonds, and K. Keay (2010), Mesoscale cyclone activity over the ice-free Southern Ocean: 1999-2008, *Journal Climate*, 23, 5404–5420, doi: 10.1175/2010JCLI3628.1

Jones, C. R., C. S. Bretherton, and D. Leon, (2011), Coupled vs. decoupled boundary layers in VOCALS-REx. *Atmospheric Chemistry and Physics*, 11, 7143–7153, https://doi:10.5194/acp-11-7143-2011

Jensen, J. B., Lee, S., Krummel, P. B., Katzfey, J., & Gogoasa, D. (2000), Precipitation in marine cumulus and stratocumulus. Part I: Thermodynamic and dynamic observations of closed cell circulations and cumulus bands. *Atmospheric Research*, 54(2), 117–155. https://doi.org/10.1016/S0169-8095(00)00040-5

Klein, S. A., and D. L. Hartmann, 1993, The seasonal cycle of low stratiform clouds. *Journal Climate*, 6, 1587–1606, https://doi.org/ 10.1175/1520-0442(1993)006,1587:TSCOLS.2.0.CO;2

Lang, F., Huang, Y., Siems, S. T., & Manton, M. J. (2018), Characteristics of the marine atmospheric boundary layer over the Southern Ocean in response to the synoptic forcing. *Journal of Geophysical Research: Atmospheres*, 123, 7799—7820. https://doi.org/10.1029/2018JD028700

Lim, E.-P. & Simmonds, I (2007), Southern Hemisphere winter extratropical cyclone characteristics and vertical organization observed with the ERA-40 data in 1979–2001. *Journal Climate*. 20, 2675–2690. https://doi.org/10.1175/JCLI4135.1

Liu, Y., Key, J. R., Ackerman, S. A., Mace, G. G., and Zhang, Q. (2012), Arctic cloud macrophysical characteristics from CloudSat and CALIPSO, *Remote Sensing of Environment*, 124, 159–173. https://doi.org/10.1016/j.rse.2012.05.006

Luo, Y., Xu, K.-M., Morrison, H., McFarquhar, G. M., Wang, Z., and Zhang, G. (2008), Multi-layer Arctic mixed-phase clouds simulated by a cloud-resolving model: Comparison with ARM observations and sensitivity experiments, *Journal of Geophysical Research: Atmospheres*, 113, D12208, https://doi.org/10.1029/2007JD009563, 2008

Mace, G. G., and A. Protat, (2018), Clouds over the Southern Ocean as observed from the R/V Investigator during CAPRICORN. Part II: The properties of nonprecipitating stratocumulus. *Journal of Applied Meteorology and Climatology*, 57, 1805–1823, https://doi.org/10.1175/JAMC-D-17-0195.1

Mace, G. G., Zhang, Q., Vaughan, M., Marchand, R., Stephens, G., Trepte, C., & Winker, D. (2009), A description of hydrometeor layer occurrence statistics derived from the first year of merged Cloudsat and CALIPSO data. *Journal of Geophysical Research: Atmospheres*, 114, D00A26. https://doi.org/10.1029/2007JD009755

Mason, S., C. Jakob, A. Protat, and J. Delanoë, 2014: Characterizing observed midtopped cloud regimes associated with Southern Ocean shortwave radiation biases. *Journal of Climate*, 27, 6189–6203, doi:10.1175/JCLI-D-14-00139.1.

Muhlbauer, A., McCoy, I. L., & Wood, R. (2014), Climatology of stratocumulus cloud morphologies: Microphysical properties and radiative effects. *Atmospheric Chemistry and Physics*, 14(13), 6695–6716

Murray, R. J., and I. Simmonds, (1991), A numerical scheme for tracking cyclone centres from digital data. Part I: Development and operation of the scheme. *Meteorology of the Southern Hemisphere*, 39, 155–166

Naud, C. M., Booth, J. F., & DelGenio, A. D. (2016), The relationship between boundary layer stability and cloud cover in the post-cold-frontal region. *Journal Climate*, 29(22), 8129–8149. https://doi.org/10.1175/JCLI-D-15-0700.1

Naud, C. M., Posselt, D. J., & vanden Heever, S. C. (2015), A CloudSat–CALIPSO view of cloud and precipitation properties across cold fronts over the global oceans. *Journal Climate*, 28(17), 6743–6762. https://doi.org/10.1175/JCLI-D-15-0052.1

Naud, C.M., Booth, J. F., & Del Genio, A. D. (2014), Evaluation of ERA-Interim and MERRA cloudiness in the Southern Ocean. *Journal Climate*, 27(5), 2109–2124. https://doi.org/10.1175/JCLI-D-13-00432.1

Nicholls, S. and Turton, J. (1986), An observational study of the structure of stratiform cloud sheets. 2. Entrainment, *Quarterly Journal of the Royal Meteorological Society*, 112, 461–480. https://doi.org/10.1002/qj.49711247210

Parish, T. R. and Cassano, J. J. (2003), The role of katabatic winds on the Antarctic surface wind regime. *Monthly Weather Review*, 131, 317–333

Pezza, A. B., T. Durrant, I. Simmonds, and I. Smith (2008), Southern Hemisphere synoptic behavior in extreme phases of SAM, ENSO, sea ice extent and southern Australia rainfall, *Journal Climate*, 21, 5566-5584

Rudeva, I., I. Simmonds, D. Crock, and G. Boschat (2019), Midlatitude fronts and variability in the Southern Hemisphere tropical width, *Journal Climate*, 32, 8243-8260, doi: 10.1175/JCLI-D-18-0782.1.

Russell, L. M., Lenschow, D. H., Laursen, K. K., Krummel, P. B., Siems, S. T., Bandy, A. R., et al. (1998), Bidirectional mixing in an ACE 1 marine boundary layer overlain by a second turbulent layer. *Journal of Geophysical Research: Atmospheres*, 103(D13), 16,411–16, 432. https://doi.org/10.1029/97JD03437

Schemm, S., I. Rudeva, and I. Simmonds (2015), Extratropical fronts in the lower troposphere: Global perspectives obtained from two automated methods, *Quarterly Journal of the Royal Meteorological Society*, 141, 1686-1698, doi: 10.1002/qj.2471.

Schuddeboom, A., et al., 2019, Cluster-based evaluation of model compensating errors: A case study of cloud radiative effect in the Southern Ocean. *Geophysical Research Letters*, 46, 3446-3453, doi: 10.1029/2018GL081686

Simmonds, I., & K. Keay, (2000), Mean Southern Hemisphere extratropical cyclone behavior in the 40-year NCEP-NCAR reanalysis. *Journal Climate*, 13(5), 873–885. https://doi.org/10.1175/1520-0442(2000)013<0873:MSHECB>2.0.CO;2

Simmonds, I., and J. C. King (2004), Global and hemispheric climate variations affecting the Southern Ocean, *Antarctic Science*, 16, 401-413, doi: 10.1017/S0954102004002226

Simmonds, I., and E.-P. Lim (2009), Biases in the calculation of Southern Hemisphere mean baroclinic eddy growth rate, *Geophysical Research Letters*, 36, L01707, doi: 10.1029/2008GL036320

Stein, A.F., Draxler, R.R, Rolph, G.D., Stunder, B.J.B., Cohen, M.D., and Ngan, F., (2015), NOAA's HYSPLIT atmospheric transport and dispersion modeling system, *Bulletin of the American Meteorological Society*, 96, 2059-2077, http://dx.doi.org/10.1175/BAMS-D-14-00110.1

Trenberth, K. E., and J. T. Fasullo, (2010), Simulation of present-day and twenty-first-century energy budgets of the Southern Oceans. *Journal Climate*, 23, 440–454. https://doi.org/10.1175/2009JCLI3152.1

Zelinka, M. D., and D. L. Hartmann, (2012), Climate feedbacks and their implications for poleward energy flux changes in a warming climate. *Journal Climate*, 25, 608–624. https://doi.org/10.1175/JCLI-D-11-00096.1

Zeng, X., M.A. Brunke, M. Zhou, C. Fairall, N. A. Bond, and D. H. Lenschow (2004), Marine atmospheric boundary layer height over the eastern Pacific: Data analysis and model evaluation, *Journal Climate*, 17, 4159–4170, https://doi:10.1175/JCLI3190.1

Zheng, Y., & Li, Z. (2019), Episodes of warm- air advection causing cloud- surface decoupling during the MARCUS. *Journal of Geophysical Research: Atmospheres*, 124. https://doi. org/10.1029/2019JD030835

Zhou, X., Kollias, P., & Lewis, E. R. (2015), Clouds, precipitation, and marine boundary layer structure during the MAGIC field campaign. *Journal Climate*, 28(6), 2420–2442. https://doi.org/10.1175/JCLI- D- 14- 00320.1

Vassel M., Ickes L., Maturilli M., and Hoose1C., (2019), Classification of Arctic multilayer clouds using radiosonde and radar data in Svalbard. *Atmospheric Chemistry and Physics*, 19, 5111–5126, 2019. https://doi.org/10.5194/acp-19-5111-2019

Wood, R., & Bretherton, C. S. (2006), On the relationship between stratiform low cloud cover and lower-tropospheric stability. *Journal Climate*, 19(24), 6425–6432. https://doi.org/10.1175/JCLI3988.1

Williams, K. D., Bodas-Salcedo, A., Déqué, M., Fermepin, S., Medeiros, B., Watanabe, M., et al. (2013), The Transpose-AMIP II experiment and its application to the understanding of Southern Ocean cloud biases in climate models. *Journal Climate*, 26(10), 3258–3274. https://doi.org/10.1175/JCLI-D-12-00429.1

Yin, B., and B. A. Albrecht, (2000), Spatial variability of atmospheric boundary layer structure over the eastern equatorial Pacific. *Journal Climate*, 13, 1574–1592, https://doi.org/10.1175/1520-0442(2000)013,1574:SVOABL.2.0.CO;2